

RESEARCH ARTICLE

Autologous adipose-derived stem cell transplantation enhances healing of wound with exposed bone in a rat model

Tomo Hamada , Hidenori Matsubara*, Yasuhisa Yoshida , Shuhei Ugaji, Issei Nomura, Hiroyuki Tsuchiya

Department of Orthopaedic Surgery, Graduate School of Medical Sciences, Kanazawa University, Kanazawa, Japan

* seikei@med.kanazawa-u.ac.jp



Abstract

Objectives

Soft tissue wounds with exposed bone often require extended healing times and can be associated with severe complications. We describe the ability of artificial dermis with autogenic adipose-derived stem cells (ADSCs) to promote the healing of wounds with exposed bone in a rat model.

Methods

Adipose tissues harvested from the bilateral inguinal regions of Wistar rats were used as ADSCs. Rats were randomly divided into control and ADSC groups to investigate the efficacy of ADSC transplantation for wound healing ($n = 20$ per group). Soft tissue defects were created on the heads of the rats and were covered with artificial dermis with or without the seeded ADSCs. Specimens from these rats were evaluated using digital image analysis, histology, immunohistochemistry, cell labeling, and real-time reverse-transcription polymerase chain reaction (real-time RT-PCR).

Results

The average global wound area was significantly smaller in the ADSC group than in the control group on days 3, 7, and 14 after surgery ($p < 0.05$). After 14 days, the blood vessel density in the wound increased by 1.6-fold in the ADSC group compared with that in the control group ($p < 0.01$). Real-time RT-PCR results showed higher *Fgfb* and *Vegf* expression levels at all time points, and higher *Tgfb1* and *Tgfb3* expression levels until 14 days after surgery in the ADSC group than in the control group ($p < 0.05$).

Conclusions

In wounds with exposed bone, autogenic ADSCs can promote vascularization and wound healing. Use of this cell source has multiple benefits, including convenient clinical application and lack of ethical concerns.

OPEN ACCESS

Citation: Hamada T, Matsubara H, Yoshida Y, Ugaji S, Nomura I, Tsuchiya H (2019) Autologous adipose-derived stem cell transplantation enhances healing of wound with exposed bone in a rat model. PLoS ONE 14(5): e0214106. <https://doi.org/10.1371/journal.pone.0214106>

Editor: Gianpaolo Papaccio, Università degli Studi della Campania, ITALY

Received: March 4, 2019

Accepted: April 30, 2019

Published: May 13, 2019

Copyright: © 2019 Hamada et al. This is an open access article distributed under the terms of the [Creative Commons Attribution License](https://creativecommons.org/licenses/by/4.0/), which permits unrestricted use, distribution, and reproduction in any medium, provided the original author and source are credited.

Data Availability Statement: All relevant data is within the paper.

Funding: The authors received no specific funding for this work.

Competing interests: The authors have declared that no competing interests exist.

Introduction

Some wounds caused by ulcers, trauma, and various operations result in exposed bone, leading to severe complications in many cases during treatment of soft tissue. Currently, surgical treatment for defects with exposed bone typically involves the use of local or distal skin flaps, muscle flaps, or myocutaneous flaps. However, there are many risks associated with wound coverage by these flaps, and a complicated microsurgical approach is required for successful treatment. Moreover, use of a composite tissue transfer technique may not be possible in such cases owing to the paucity of the graft donor site and other factors.

Artificial dermis is a commercially available treatment for full-thickness skin defects after debridement. Clinical reports have demonstrated its successful clinical application to promote healing by creating a vascular matrix over an exposed bone [1,2]. However, the formation of neodermal tissue is delayed, thereby prolonging the treatment period. A main reason for the prolonged treatment period is the slow vascularization rate [3]. Several recent studies have shown that in the context of tissue injury, mesenchymal stem cells (MSCs) exhibit excellent potential for promoting healing and vascularization of wounds [4,5]. Among the various types of MSCs, adipose-derived stromal stem cells (ADSCs) have many unique advantages. ADSCs are abundant in the subcutaneous adipose tissue and can be easily harvested using a syringe or a minimally invasive lipoaspiration procedure. They have been shown to contribute to the complex wound-repair processes, comprising inflammation, granulation, and remodeling [6,7]. ADSCs secrete angiogenic and anti-apoptotic factors [8,9] and exhibit various advantageous properties such as paracrine activity and angiogenic potential [10–13]. Additionally, several reports have described that ADSCs show regenerative aptitudes, thereby promoting tissue repair, in several clinical fields, including plastic, orthopedic, cardiac, bone, and breast surgery [14–16].

Our aim was to evaluate the efficacy of autogenic ADSCs with artificial dermis to promote the healing and vascularization of a wound with exposed bone, which is one of the wounds with the worst healing conditions.

Methods

Animal experiments

All experimental protocols were approved by the Kanazawa University Advanced Science Research Center (Approval Number: AP-173885). Forty-three female Wistar rats [age, 8–9 weeks and mean weight, 147.4 g (\pm 9.3 g)] were used in this experiment, and housed under specific pathogen-free conditions with three rats per cage in a 12-hour light/dark cycle with ad libitum access to food and water. A schematic overview of the experimental design is shown in Fig 1. The rats were anesthetized with an intraperitoneal injection of pentobarbital (40 mg/kg) and xylazine (15 mg/kg). The adipose tissues were harvested from the bilateral inguinal region (total yield of approximately 1.2 g) for use as ADSCs. After one week, 12 \times 12-mm² circular soft tissue defects with exposed bone were created on the heads of the rats by removing the cutaneous tissue and the periosteum of the cranium using a modification of a previously reported method [17]. After creating the soft tissue defect, all rats were housed with one rat per cage. The rats were randomly divided into two groups (a control group and an ADSC group, 20 rats each) to investigate the efficacy of ADSC transplantation for wound healing. The soft tissue defects were then covered with a 12 \times 12-mm² circular artificial dermis with or without the seeded ADSCs. Defects were closed with six stitches using 5–0 monofilament nylon sutures (Keisei Medical, Tokyo, Japan), and the extent of wound healing of the defects was observed at 3, 7, 14, and 21 days after surgery (n = 5 at each time point). All rats from each

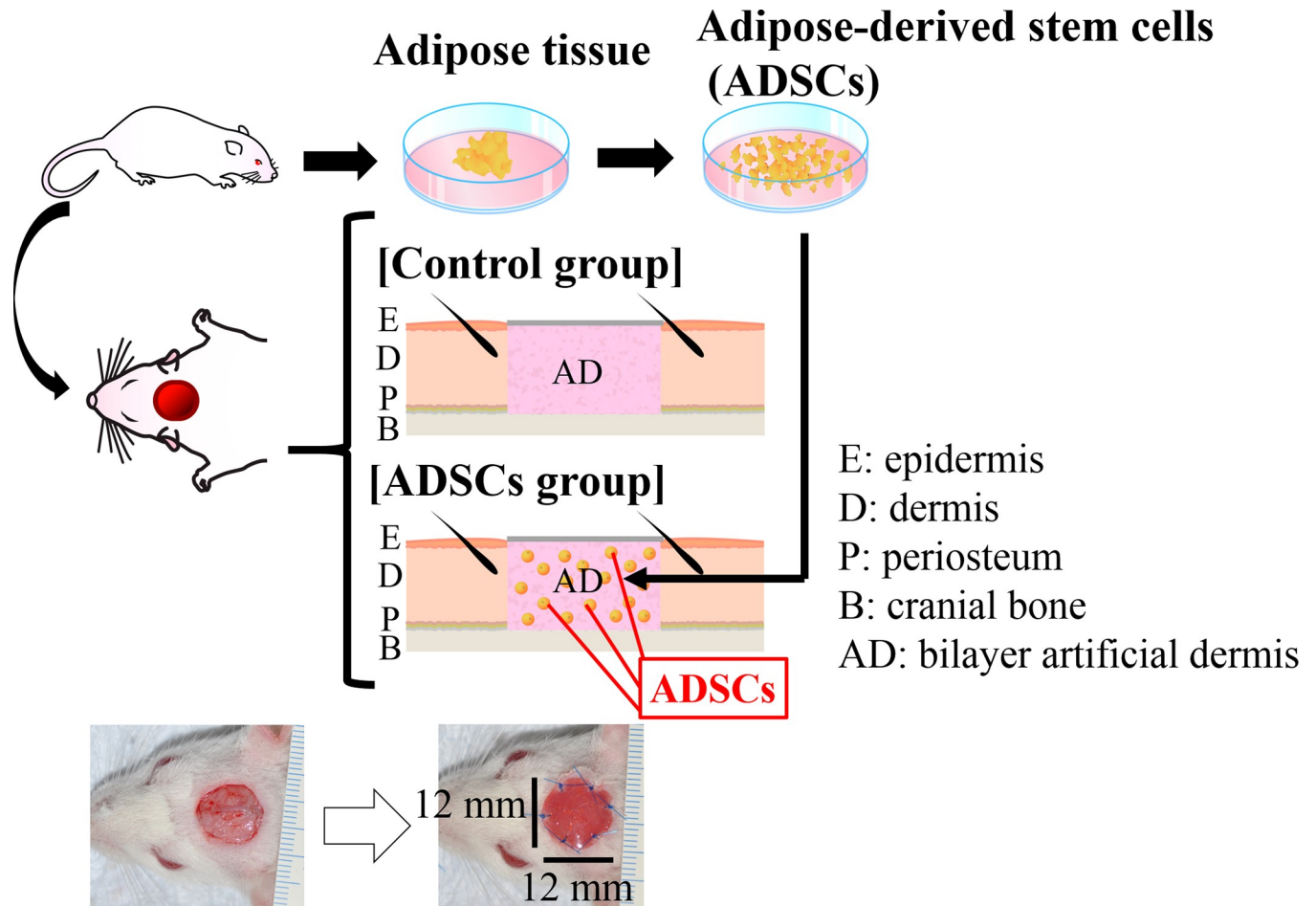


Fig 1. Schematic representation of the experimental procedure for transplanting autogenic ADSCs with an artificial dermis into a rat wound model with exposed bone. Scale bar: 1 mm.

<https://doi.org/10.1371/journal.pone.0214106.g001>

group were euthanized by intraperitoneal injection of pentobarbital (200 mg/kg) after tracing the wound area on the photograph taken at the established endpoint. The specimens from these rats were then evaluated using digital image analysis, histology, immunohistochemistry, and real-time reverse-transcription-polymerase chain reaction (RT-PCR). The three remaining rats were used for DiI labeling.

Artificial dermis

We used the commercially available artificial dermis Integra (Life Sciences Corp., Plainsboro, NJ, USA) for this experiment. Integra is widely used in the clinical treatment of deep partial-thickness and full-thickness burn wounds [18,19]. In addition, in clinical settings, Integra has been successfully used to promote healing of wounds with exposed bone [1,2].

Isolation of ADSCs

ADSCs were isolated from the bilateral inguinal adipose tissue of the rats following a modification of a previously reported method [20]. In brief, the adipose tissue was washed with phosphate-buffered saline (PBS; Fujifilm Wako Pure Chemical Corporation, Osaka, Japan) and cut into strips. Collagenase (Fujifilm Wako Pure Chemical Corporation, Osaka, Japan) was

dissolved in 20 mL of PBS to a final concentration of 0.1% to digest the adipose tissue for 60 minutes in a 37°C water bath (the mixture was shaken every 15 minutes during the digestion period). Immediately after the reaction was completed, 20 mL of Dulbecco's modified Eagle's medium (DMEM; Fujifilm Wako Pure Chemical Corporation, Osaka, Japan) was added to neutralize the collagenase activity. The resulting solution was then filtered by a 40- μ m cell strainer (Corning Inc., Corning, NY, USA), the filtrate was centrifuged at 700 \times g for 6 minutes at 25°C, and the supernatant was removed. The remaining deposit was added to DMEM supplemented with 10% fetal bovine serum (FBS; Corning Inc., Corning, NY, USA) and 1% penicillin/streptomycin (P/S; Fujifilm Wako Pure Chemical Corporation, Osaka, Japan), plated on a 60.1-cm² tissue culture dish (TPP Techno Plastic Products, Trasadingen, Switzerland), and cultured at 37°C in a 5% CO₂ incubator. After 24 hours, the debris was removed by washing with PBS, and fresh medium was added. The ADSCs were selected based on the ability of cells to adhere to the culture plate. The cells were passaged with 0.25% trypsin-ethylenediaminetetraacetic acid (Fujifilm Wako Pure Chemical Corporation, Osaka, Japan) on day 3 and transferred to a new dish. Cells were used at the third passage in all experiments. Kato et al. [21] proved that these cells have MSC-like self-renewal, adipogenesis, and osteogenesis properties.

ADSC seeding

Integra was placed with the silicone side positioned downward. In this scaffold, 1.0×10^6 ADSCs/mL were seeded drop-wise with 40 μ L of DMEM supplemented with 10% FBS and 1% P/S according to the fluid capacity of the scaffold. The scaffold of the control group was placed in a separate tissue culture dish with the same culture medium but without ADSCs. All dishes were incubated at 37°C with 5% CO₂. After 24 hours, just prior to transplanting, the debris was removed by washing with PBS, and fresh medium was added.

Wound area

On the day of surgery and at the established endpoints (3, 7, 14, and 21 days after surgery), the wound area was measured by tracing the wound margin on the photograph followed by calculation of the pixel data using ImageJ software (National Institutes of Health, Bethesda, MD, USA). The global wound area (%) was calculated according to the residual wound area on a given day (tx) relative to the wound area measured on the day of surgery, as follows:

$$\text{Global wound area} = \frac{[\text{tx wound area}]}{[\text{original wound area}]} \times 100$$

Histological analysis of paraffin-embedded tissues

At the established endpoints (3, 7, 14, and 21 days after surgery), the wounds were harvested with approximately 5-mm margins and the cranial bone attached ($n = 5$ at each time point). A part (right quarter) of the wound was used for subsequent real-time RT-PCR analysis. The remaining part of the wound was fixed in 10% neutralized formalin solution and dehydrated using an ethanol gradient (70%, 80%, 90%, and 100%). The fixed specimens were decalcified in 10% formic sodium citrate solution, embedded in paraffin, and sectioned in the coronal plane. The sections were stained with hematoxylin and eosin and Masson's trichrome, and the slides were observed using an optical microscope (Biorevo BZ-9000; Keyence Co., Osaka, Japan).

Immunohistochemistry

Tissue samples were embedded in paraffin and sectioned in the coronal plane, and the blood vessel density was analyzed immunohistochemically ($n = 5$ at 14 days after surgery per group).

Blood vessel endothelial cells were immunohistochemically stained with an anti-CD31 antibody (Abcam, Cambridge, Britain, ab28364, 1:50). The sections were incubated in Liberate Antibody Binding Solution (LAB solution; Polysciences, Philadelphia, PA, USA) at room temperature for 15 minutes, and then Protein Block Serum-Free (Dako, Glostrup, Denmark) and phosphate buffer containing hydrogen peroxide (Peroxidase-Blocking Solution, Dako, Glostrup, Denmark) were added to the sections for 10 minutes each for blocking. Primary anti-CD31 antibody in Tris-HCl buffer containing stabilizing protein and 0.015 mol/L sodium azide (Dako Antibody Diluent, Dako, Glostrup, Denmark) were then added to the slides, which were incubated at 4°C overnight. After addition of the secondary antibody, Dako REAL EnVision/HRP, Rabbit/Mouse (ENV, Dako, Glostrup, Denmark), the slides were further incubated for 30 minutes at room temperature. The samples were developed with DAB chromogen (Dako REAL DAB+ Chromogen, Dako, Glostrup, Denmark) and the substrate and observed under the microscope. Once the desired signal-to-noise ratio was achieved, the reaction was stopped by washing the slides in deionized water. To quantify vascularization within the wound, the blood vessel densities of five animals in each group at 14 days after surgery were determined by measuring the vascular area in the wound area of the specimen.

The blood vessel densities were quantified at the established endpoints in the immunohistochemically stained samples. Quantification was performed in five randomly selected high-power fields of five non-consecutive tissue sections per wound within each group [22]. Only vessels with a diameter < 50 µm [23] were considered for this analysis. In this study, it was inevitable that the collagen of the artificial dermis would become stained with an anti-CD31 antibody. Therefore, we excluded this area for measurement of the vascular area. The vessel area in the selected field of each specimen was observed with a fluorescence microscope (U-RFL-T; Olympus, Tokyo, Japan), and the images were analyzed with ImageJ software (National Institutes of Health, Bethesda, MD, USA). The percentage of the relative area of CD31-positive vessels was calculated using ImageJ software from the following equation for each time point (tx):

$$\text{Blood vessel density(\%)} = \frac{[\text{tx area of CD31 positive vessels}]}{[\text{total field area}]} \times 100$$

DiI labeling

To confirm survival potential and location of the transplanted ADSCs, the ADSCs were labeled with the fluorescent dye DiI (Vybrant DiI Cell Labeling Solution; Life Technologies, Carlsbad, CA, USA) prior to transplantation. DiI binds to cellular thiols and has long-term stability, which enables the tracing of DiI-labeled transplanted cells in the host tissue. This experiment involved a separate group of rats (n = 3). The concentration of ADSCs was adjusted to 1.0×10^6 cells/mL, and 5 µL/mL of DiI was dissolved in this medium and incubated for 15 minutes at 37°C in a 5% CO₂ incubator for ADSC labeling. After the reaction was completed, the filtrate was centrifuged at 1000 rpm for 5 minutes at 25°C, and the supernatant was removed. Once the DiI was completely removed from the filtrate, ADSCs were centrifuged twice with DMEM under the same setting, and the supernatant was removed. DiI-labeled ADSCs were seeded to the Integra scaffold and transplanted as described above. At day 21 after transplantation of the labeled ADSCs, a frozen section was prepared using Kawamoto's film method [24] in the coronal plane. The survival of the transplanted cells was then determined in the unstained samples.

Real-time RT-PCR

RNA was extracted from the granulation tissue of the rats using a NucleoSpin RNA II kit (Takara Bio, Otsu, Japan). Each sample was harvested from the right quarter of a wound with

approximately 5-mm margins without the cranial bone, and was disrupted and homogenized using a syringe (n = 5 at each time point per group). The absorbance of the resulting total RNA concentrations was determined on an ultraviolet-visible spectrophotometer with absorbance read at 260/280 nm (NanoDrop Lite; Thermo Scientific, Waltham, MA, USA). For real-time RT-PCR, 6 µg of mRNA was reverse-transcribed with RevertAid First-Strand cDNA Synthesis Kit (Thermo Scientific, Waltham, MA, USA) using a thermal cycler (T100TM Thermal Cycler; Bio-Rad, Hercules, CA, USA). Real-time RT-PCR was then carried out on an ABI Prism 7900 apparatus (Applied Biosystems, Foster City, CA, USA) using Sybr Green PCR Master Mix (Applied Biosystems, Foster City, CA, USA) per the manufacturer's instructions. Primers for rat glyceraldehyde-3-phosphate dehydrogenase (*Gapdh*), basic fibroblast growth factor (*Fgfb*), vascular endothelial growth factor (*Vegf*), transforming growth factor beta 1 (*Tgfb1*), and beta 3 (*Tgfb3*) were purchased from Hokkaido System Science Co., Ltd. Japan; the sequences are listed in Table 1. The amplification parameters were an initial 95°C incubation step for 15 minutes, followed by 20 amplification cycles of 94°C for 15 seconds, 60°C for 30 seconds, and 72°C for 30 seconds. The reactions ended with a 72°C extension step for 7 minutes, followed by storage at 4°C overnight. The expression levels of each target gene were calculated relative to the level of *Gapdh* for each sample.

Statistical analysis

All statistical analyses were performed using the Statistical Package for Social Sciences version 23.0 (SPSS, Inc., Chicago, IL, USA). All results are presented as the mean ± standard deviation (SD). The data were normally distributed; comparisons between two groups (i.e., control vs. ADSCs) in the global wound area, the percentage of the relative area of CD31-positive vessels, and relative gene expression levels were performed using Student's *t*-test; $p < 0.05$ was considered statistically significant.

Results

Global wound area

Digital photographs were obtained immediately following surgery and at 3, 7, 14, and 21 days after surgery (Fig 2A). The average global wound area was significantly smaller in the ADSC group than in the control group on days 3, 7, and 14 after surgery (Fig 2B). However, there was no significant difference between the two groups at day 21 because the wounds in almost all the rats were completely cured at that point (Fig 2B).

Table 1. Sequences of primers used in real-time RT-PCR amplification.

Primer	Sequence (5'-3')	Amplicon size (bp)
rat <i>Gapdh</i> forward	TGCACCACCAACTGCTTA	18
rat <i>Gapdh</i> reverse	GGATGCAGGGATGATGTTTC	19
rat <i>Fgfb</i> forward	GCGACCCACACGTCAAACCTA	20
rat <i>Fgfb</i> reverse	CAGCCGTCCATCTTCCTTCA	20
rat <i>Vegf</i> forward	AAATCCTGGAGCGTTCACGTGTG	22
rat <i>Vegf</i> reverse	AACGCGAGTCTGTGTTTTTGC	21
rat <i>Tgfb1</i> forward	GACCGCAACAACGCAATCTA	20
rat <i>Tgfb1</i> reverse	CACTGCTTCCCGAATGTCTGA	21
rat <i>Tgfb3</i> forward	TACTGCTTCCGCAACTTGGGA	20
rat <i>Tgfb3</i> reverse	AGGTTCTGGACCCATTTCC	20

<https://doi.org/10.1371/journal.pone.0214106.t001>

Histology

In magnified microphotographs of sagittal sections of hematoxylin and eosin-stained specimens collected 3 days after surgery (Fig 3A and 3B), inflammatory cells, mainly neutrophils, as well as red blood cells were observed within the collagen sponges in both groups. The number of cells was higher in the ADSC group than in the control group. Seven days after the surgery (Fig 3C and 3D), fibroblasts were observed in the collagen sponges with slight vascularization, and the fibroblast numbers and tissue density were higher in the ADSC group than in the control group. Fourteen days after the surgery (Fig 3E and 3F), a thick and dense dermal layer was observed in both groups. At 21 days after the surgery (Fig 3G and 3H), most of the wounds showed epithelization both macroscopically and histologically.

In Masson's trichrome-stained sections, especially at 7 and 14 days (Fig 4C–4F), higher-density granulation tissue was noted for the ADSC groups. In addition, the wounds of the ADSC groups showed greater tissue thickness and more homogeneous granulation tissue than those of the control groups at all time points (Fig 4).

Immunohistochemistry

The blood vessel density was quantified 14 days after surgery. The extent of neovascularization in the injured tissues was evaluated by immunostaining detection of CD31-expressing endothelial cells in paraffin-embedded tissue samples sectioned in the coronal plane (Fig 5A–5D). The blood vessel density in the wound was increased by 1.6-fold in the ADSC group compared with that in the control group after 14 days, representing a statistically significant difference ($p < 0.01$) (Fig 5E).

DiI labeling

Magnified microphotographs of sagittal sections of hematoxylin and eosin-stained specimens that were collected from the ADSC group 21 days after surgery are shown in Fig 6A. Histologically,

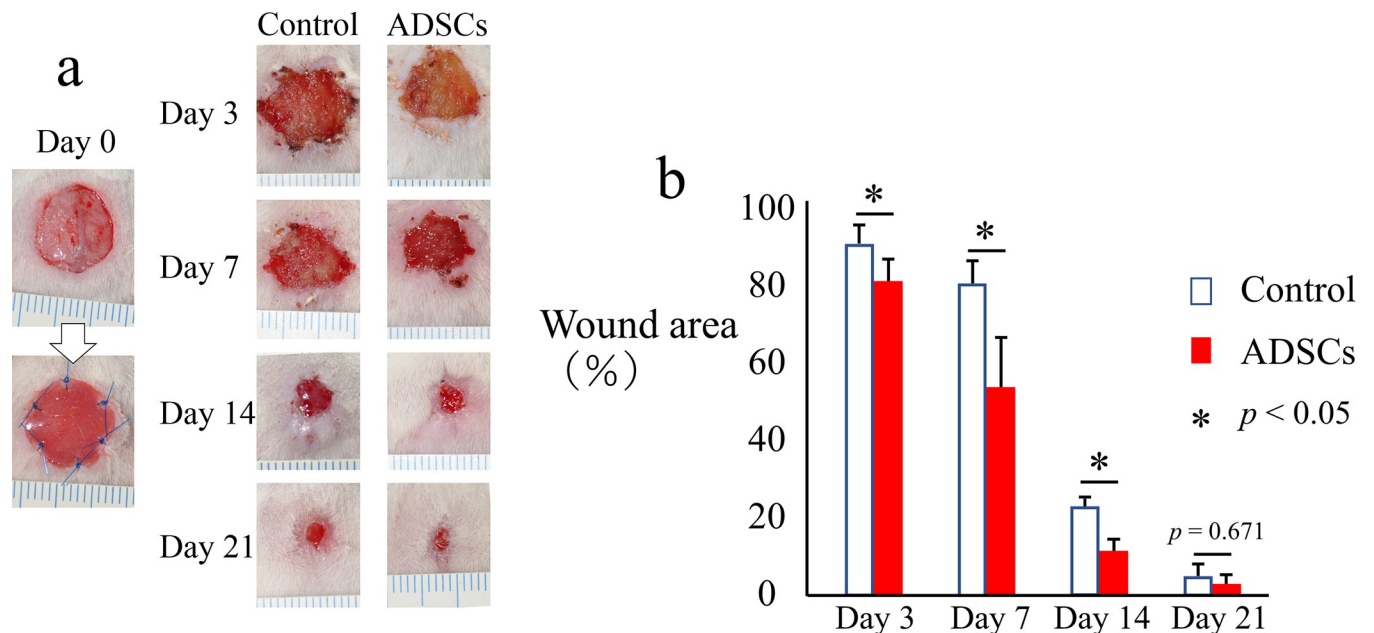


Fig 2. Images of wounds with exposed bone and comparison of healing with and without ADSC transplantation. (a) Macroscopic images of the wound with exposed bone. Scale bar: 1 mm. (b) Measurement and analysis of the wound area with or without ADSC transplantation. The data represent the mean \pm SD. * $p < 0.05$.

<https://doi.org/10.1371/journal.pone.0214106.g002>

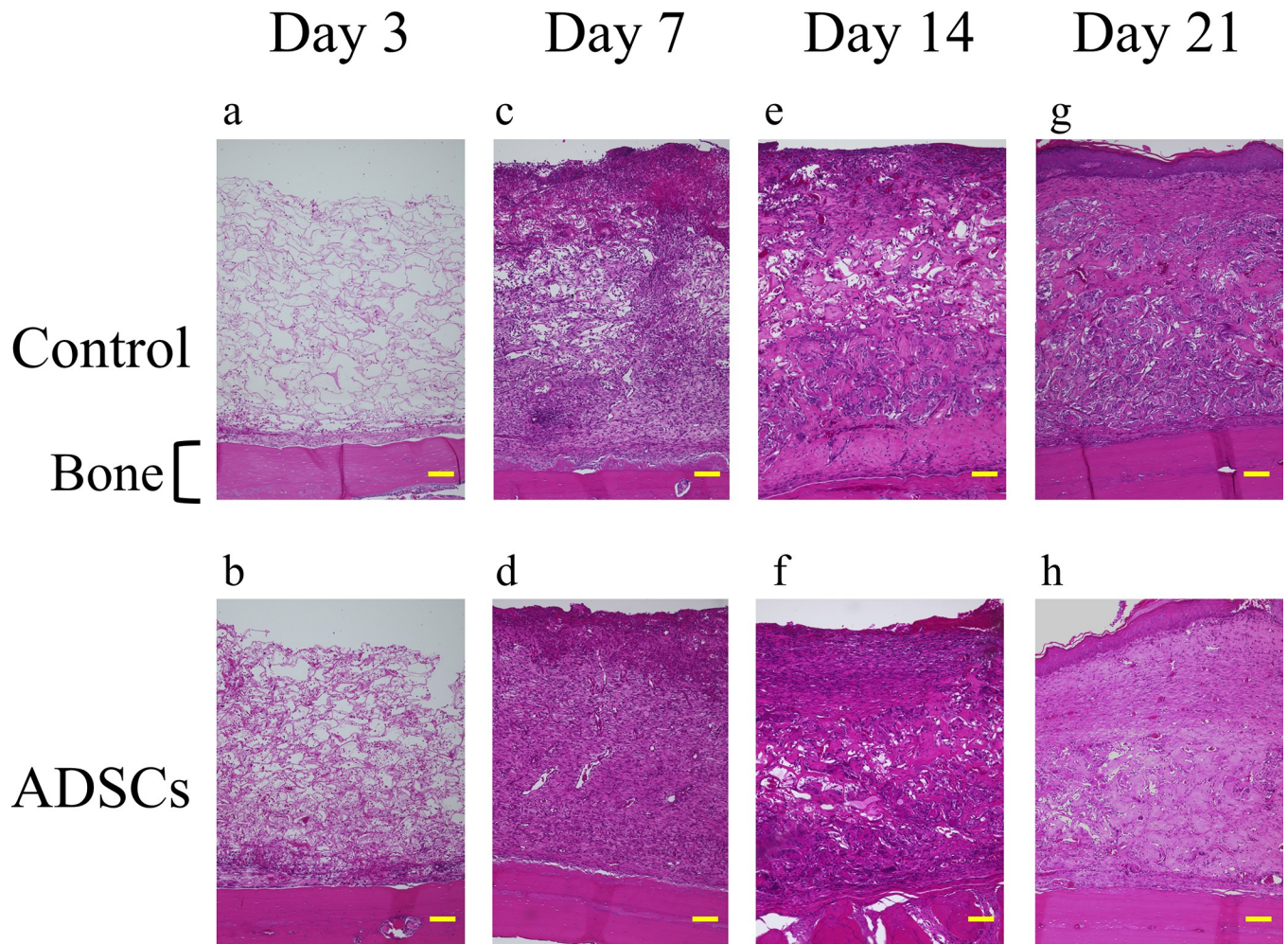


Fig 3. Representative magnified images (100x) of hematoxylin and eosin-stained histological sections of the center of the wound along with implantation time. Histological sections at day 3, 7, 14, and 21 highlight the wound healing progression along the experimental time frame. Scale bars indicate 100 μ m for all panels.

<https://doi.org/10.1371/journal.pone.0214106.g003>

most wounds showed epithelization, and high-density granulation and homogeneous tissue were noted under the epithelization. For identification of tissues using DiI labeling, the gray-scale values of the DiI-labeled section were used (Fig 6B). In the DiI-labeled section, at 21 days after surgery, numerous DiI-positive (red) cells were distributed throughout the granulation tissue (Fig 6C and 6D).

Real-time RT-PCR

The ability of the transplanted ADSCs to promote neovascularization at the molecular level was assessed based on the expression of *Fgfb* and *Vegf* using real-time RT-PCR. Significantly higher expression levels of both genes were detected at all time points for the ADSC group than for the control group ($p < 0.05$) (Fig 7).

Moreover, the expression levels of *Tgfb1* and *Tgfb3* were examined to determine the potential biomechanical effect of ADSCs that could affect extracellular matrix deposition, organization, and scarring. Significantly higher expression levels of both genes were detected in the ADSC group until 14 days after surgery than in the control group (Fig 7).

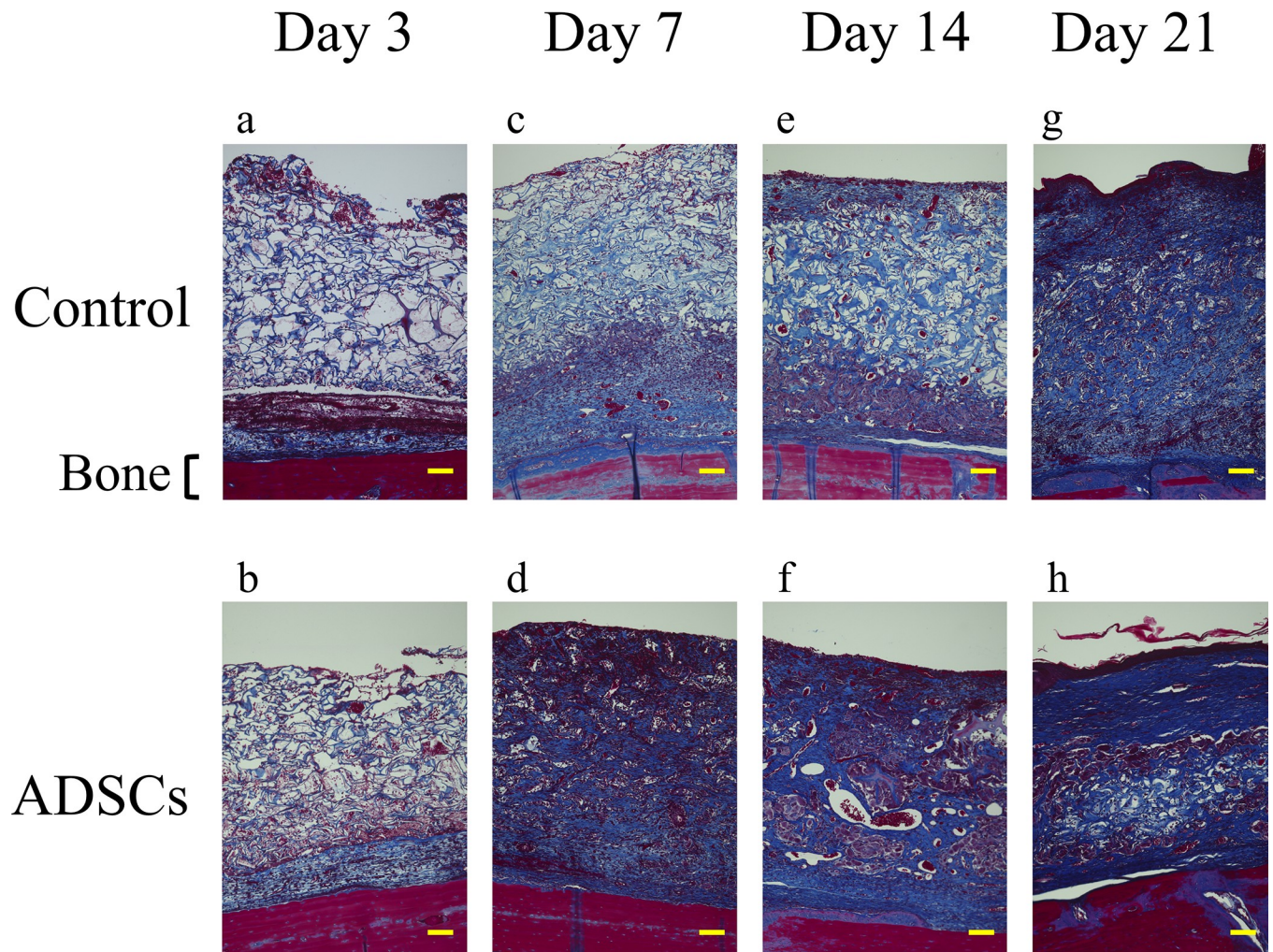


Fig 4. Representative magnified images (100x) of Masson's trichrome-stained histological sections of the center of the wound along with implantation time. Histological sections at day 3, 7, 14, and 21 highlight the wound healing progression along the experimental time frame. Scale bars indicate 100 μ m for all panels.

<https://doi.org/10.1371/journal.pone.0214106.g004>

Discussion

To our knowledge, this is the first report on the use of autogenic ADSCs with artificial dermis for healing wounds with exposed bone. The regeneration and introduction of capillaries inside the wound are important for wound healing because tissue regeneration requires blood flow to supply oxygen and nutrition and remove waste. However, wounds with exposed bone are strongly deficient in blood flow. In this study, we demonstrated that ADSCs increased the blood vessel density in the wound. Several studies have indicated that ADSCs improve the healing rate of ischemic wounds such as burn wounds [25,26], radiation ulcers [27], or diabetic wounds [21,28]. Consistent with these previous findings, we showed that application of ADSCs resulted in significantly faster reduction in the wound area. The increased blood vessel density at the ischemic wound site might be responsible for improving the wound healing rate in cases with exposed bone.

While the potential of MSCs to differentiate in vitro is widely reported [29–34], only a few studies have explored the in vivo differentiation potential of ADSCs. Cao et al. [35]

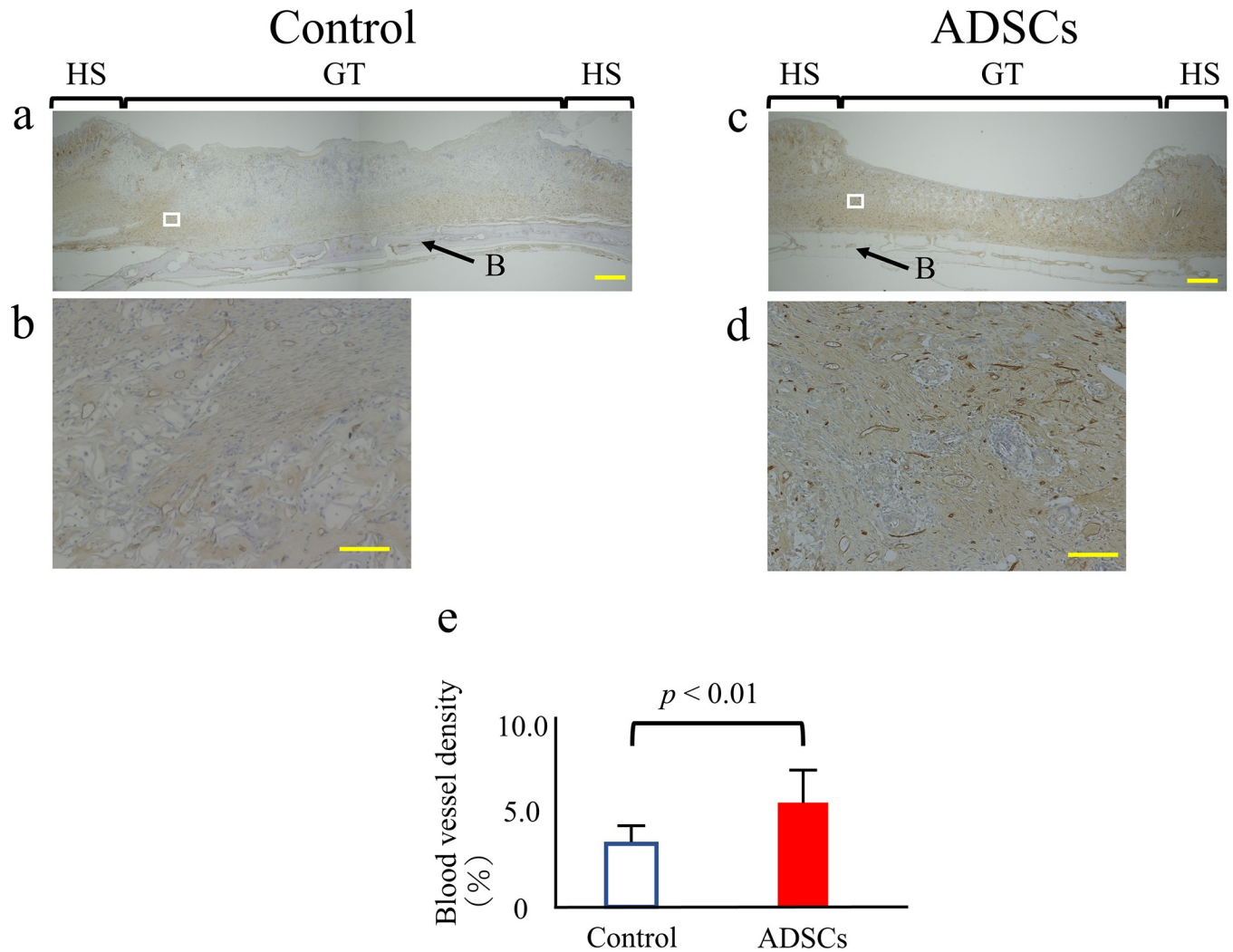


Fig 5. Quantitative analysis of wound neovascularization. (a-d) Control and ADSC specimens at 14 days after surgery were stained for CD31, a blood vessel endothelial cell marker (brown) (a, c: 40x magnification. Scale bars = 1 mm). For each group, the figure below is a higher-magnification micrograph of the boxed region in the figure above (b, d: 400x magnification. Scale bars = 100 μ m). (e) Blood vessel density was calculated by dividing the area of CD31-positive vessels by the total area. The data represent the mean \pm SD. HS = healthy skin; GT = granulation tissue; B = cranial bone.

<https://doi.org/10.1371/journal.pone.0214106.g005>

demonstrated that ADSCs express endothelial markers in vitro and, in response to local signals, can differentiate into endothelial cells that contribute to neoangiogenesis in ischemia models. Lu et al. [36] demonstrated that endothelial cells of the capillary are DiI positive (ADSCs) and that ADSCs enhanced the blood supply to skin flaps in an animal model both directly, via differentiation into endothelial cells, and indirectly, through modulation of angiogenic growth factors. The results of the present study might not be sufficient to state that ADSCs directly differentiated into endothelial cells because we could not clearly determine the form, nature, or detailed locations of the DiI-positive cells. However, we observed the continued presence of numerous DiI-positive ADSCs distributed throughout the granulation tissue up to 21 days post-transplantation (Fig 4C). This result suggests that ADSCs might differentiate into other cell types, such as fibroblasts or blood vessel endothelial cells. Moreover, in terms of paracrine activity and angiogenic potential, the significantly higher expression of Fgfb and Vegf in the ADSC group than in the control group elicited improved neovascularization

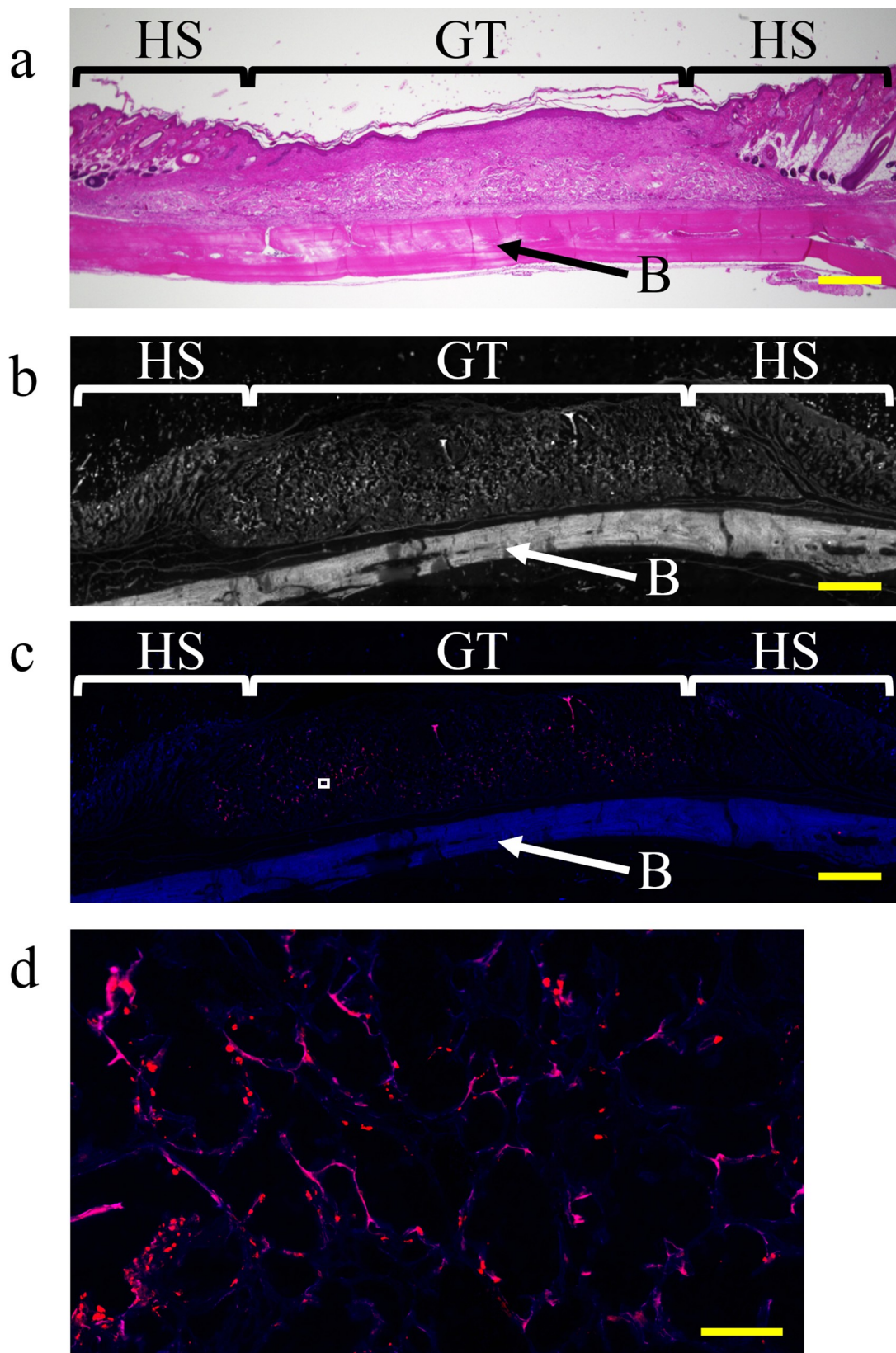


Fig 6. Representative images of DiI labeling of the center of the wound along with implantation time. Frozen sections were prepared at 21 days after transplantation of ADSCs labeled with DiI dye. (a) Magnified microphotographs of sagittal sections of hematoxylin and eosin-stained specimens collected from the ADSC group 21 days after surgery. (b) Grayscale values of frozen sections of each tissue (40× magnification); these values were similar to those for the frozen section in (c). Scale bar, 1 mm. (c) Frozen section with DiI labeling (40× magnification. Scale bar, 1 mm). (d) High-magnification image (500×) of the boxed region in (c). Scale bar, 100 μm. HS = healthy skin; GT = granulation tissue; B = cranial bone.

<https://doi.org/10.1371/journal.pone.0214106.g006>

in the ADSC group. *Fgfb* and *Vegf* are known to play important roles in wound healing and can be secreted by ADSCs, thereby influencing neovascularization [37,38]. In a previous study, significantly higher expression of *Fgfb* and *Vegf* was detected when a full-thickness excisional wound was treated with ADSCs [39]. In full-thickness excisional wounds (without exposed bone), ADSCs exhibited increased *Tgfb3* expression, decreased the scar size, and facilitated better collagen organization, scar pliability, and a more mature collagen arrangement [38,40]. Further, Zonari et al. [39] reported that the use of artificial dermis with ADSCs reduced *Tgfb1* expression in full-thickness excisional wounds. *Tgfb3* was previously found to promote normal collagen organization [38,41]. However, *Tgfb1* overexpression resulted in excessive fibroblast migration, myfibroblast differentiation, and scar formation [42]. In this study, significantly higher expression levels of both *Tgfb1* and *Tgfb3* were observed in the ADSC group than in the control group. We believe that, in wounds with exposed bone, higher expression levels of both *Tgfb1* and *Tgfb3* are desirable for covering the bone surface. Our data demonstrated that ADSCs exhibited increased expression of both *Tgfb1* and *Tgfb3* in wounds with exposed bone

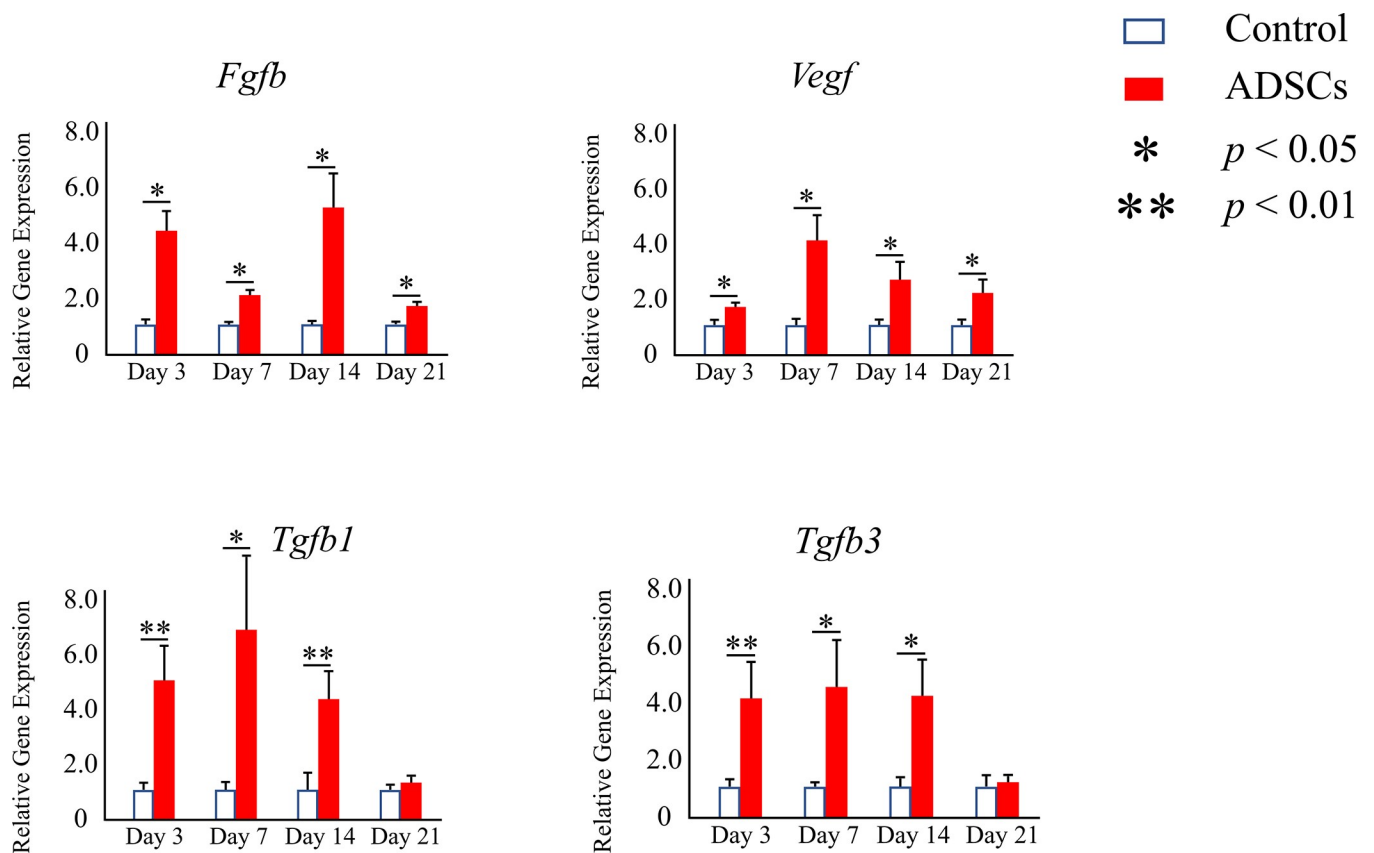


Fig 7. Relative expression levels of *Fgfb*, *Vegf*, *Tgfb1*, and *Tgfb3* among the different groups at different time points of implantation determined using real-time RT-PCR. The data represent the mean ± SD. * $p < 0.05$, ** $p < 0.01$.

<https://doi.org/10.1371/journal.pone.0214106.g007>

and promoted both scar formation and normal collagen organization for covering the bone surface.

The present study has two limitations. The first limitation is that wound-healing mechanisms are different between humans and rodents. Humans display re-epithelialization and granulation tissue formation-based wound healing, whereas rats or mice exhibit contraction-based wound healing. Therefore, in a rodent model of full-thickness excisional wound of the back, some studies use silicone rings around the wound to reduce contraction upon wounding, thus allowing a system more representative of human wound healing [6,43]. However, in our model, using silicone rings is difficult; moreover, they result in serious stress to the model. In this study, artificial dermis was placed on a wound and fixed with nylon threads to reduce wound contraction and prevent wound enlargement as a result of the loose skin of the rats. The second limitation of the study is that direct protein expression was not assessed. We identified the factors promoting neovascularization using real-time RT-PCR and confirmed the findings by CD31 immunostaining. However, we did not directly measure the proteins encoded by the identified mRNAs. We plan to analyze the expression of these proteins in subsequent studies.

Conclusions

In this study, to facilitate clinical application, we used ADSCs that were simply seeded drop-wise with a medium, along with the artificial dermis Integra that is commonly used as a scaffold. Further, in this study, we used autogenic ADSCs that have several important advantages regarding the convenience of their clinical application and fewer ethical concerns compared with those for allogeneic or xenogeneic ADSCs. Although a potential limitation to the translational use of ADSCs in patients is the enzymatic isolation technique used, we think that this technology is highly clinically translatable since both ADSCs and artificial dermis are relatively easy to obtain. Our study represents the first report that an existing artificial dermis can maintain autogenic ADSCs, which can promote the vascularization capacity and enhance wound healing in a wound with exposed bone.

Acknowledgments

We thank Ms. Yoko Kasai for her skillful technical assistance in the immunohistochemical analysis of paraffin-embedded tissues.

Author Contributions

Conceptualization: Tomo Hamada.

Data curation: Tomo Hamada.

Formal analysis: Tomo Hamada.

Funding acquisition: Tomo Hamada, Hidenori Matsubara, Yasuhisa Yoshida.

Investigation: Tomo Hamada.

Methodology: Tomo Hamada, Hidenori Matsubara, Issei Nomura.

Project administration: Tomo Hamada.

Resources: Tomo Hamada.

Software: Tomo Hamada.

Supervision: Tomo Hamada, Hidenori Matsubara, Hiroyuki Tsuchiya.

Validation: Tomo Hamada, Hidenori Matsubara, Yasuhisa Yoshida, Shuhei Ugaji, Issei Nomura.

Visualization: Tomo Hamada.

Writing – original draft: Tomo Hamada.

Writing – review & editing: Tomo Hamada.

References

1. Lee LF, Porch JV, Spenler W, Garner WL. Integra in lower extremity reconstruction after burn injury. *Plast Reconstr Surg.* 2008; 121(4): 1256–1262. <https://doi.org/10.1097/01.prs.0000304237.54236.66> PMID: 18349644
2. Molnar JA, DeFranzo AJ, Hadaegh A, Morykwas MJ, Shen P, Argenta LC. Acceleration of Integra incorporation in complex tissue defects with subatmospheric pressure. *Plast Reconstr Surg.* 2004; 113(5): 1339–1346. PMID: 15060345
3. Jones I, Currie L, Martin R. A guide to biological skin substitutes. *Br J Plast Surg.* 2002; 55(3): 185–193. <https://doi.org/10.1054/bjps.2002.3800> PMID: 12041969
4. Murphy MB, Moncivais K, Caplan AI. Mesenchymal stem cells: environmentally responsive therapeutics for regenerative medicine. *Exp Mol Med.* 2013; 45: e54. <https://doi.org/10.1038/emm.2013.94> PMID: 24232253
5. Teng M, Huang Y, Zhang H. Application of stems cells in wound healing—an update. *Wound Repair Regen.* 2014; 22(2): 151–160. <https://doi.org/10.1111/wrr.12152> PMID: 24635168
6. Martin PM, Maux A, Laterreur V, Mayrand D, Gagné VL, Moulin VJ, et al. Enhancing repair of full-thickness excisional wounds in a murine model: impact of tissue-engineered biological dressings featuring human differentiated adipocytes. *Acta Biomater.* 2015; 22: 39–49. <https://doi.org/10.1016/j.actbio.2015.04.036> PMID: 25934321
7. Broughton G, Janis JE, Attinger CE. The basic science of wound healing. *Plast Reconstr Surg.* 2006; 117(7 Suppl): 12S–34S. <https://doi.org/10.1097/01.prs.0000225430.42531.c2> PMID: 16799372
8. Rehman J, Traktuev D, Li J, Merfeld-Clauss S, Temm-Grove CJ, Bovenkerk JE, et al. Secretion of angiogenic and antiapoptotic factors by human adipose stromal cells. *Circulation.* 2004; 109(10): 1292–1298. <https://doi.org/10.1161/01.CIR.0000121425.42966.F1> PMID: 14993122
9. Schäffler A, Büchler C. Concise review: adipose tissue-derived stromal cells—basic and clinical implications for novel cell-based therapies. *Stem Cells.* 2007; 25(4): 818–827. <https://doi.org/10.1634/stemcells.2006-0589> PMID: 17420225
10. Casteilla L, Planat-Benard V, Laharrague P, Cousin B. Adipose-derived stromal cells: their identity and uses in clinical trials, an update. *World J Stem Cells.* 2011; 3(4): 25–33. <https://doi.org/10.4252/wjsc.v3.i4.25> PMID: 21607134
11. Kern S, Eichler H, Stoeve J, Klüter H, Bieback K. Comparative analysis of mesenchymal stem cells from bone marrow, umbilical cord blood, or adipose tissue. *Stem Cells.* 2006; 24(5): 1294–1301. <https://doi.org/10.1634/stemcells.2005-0342> PMID: 16410387
12. Na J, Song SY, Kim JD, Han M, Heo JS, Yang CE, et al. Protein-Engineered Large Area Adipose-derived Stem Cell Sheets for Wound Healing. *Sci Rep.* 2018; 8(1): 15869. <https://doi.org/10.1038/s41598-018-34119-x> PMID: 30367098
13. Paino F, La Noce M, Di Nucci D, Nicoletti GF, Salzillo R, De Rosa A, et al. Human adipose stem cell differentiation is highly affected by cancer cells both in vitro and in vivo: implication for autologous fat grafting. *Cell Death Dis.* 2017; 8(1): e2568. <https://doi.org/10.1038/cddis.2016.308> PMID: 28102844
14. Gimble MJ, Bunnell BA, Guilak F. Human adipose-derived cells: an update on the transition to clinical translation. *Regen Med.* 2012; 7: 225–235. <https://doi.org/10.2217/rme.11.119> PMID: 22397611
15. Kozlik M, Wójcicki P. The use of stem cells in plastic and reconstructive surgery. *Adv Clin Exp Med.* 2014; 23: 1011–1017. <https://doi.org/10.17219/acem/37360> PMID: 25618130
16. Longo UG, Rizzello G, Berton A, Ciuffreda M, Migliorini F, Khan WS, et al. Potential of adipose derived stem cells in orthopaedic surgery. *Curr Stem Cell Res Ther.* 2013; 8: 418–421. PMID: 24016327
17. Koga Y, Komuro Y, Yamato M, Sueyoshi N, Kojima Y, Okano T, et al. Recovery course of full-thickness skin defects with exposed bone: an evaluation by a quantitative examination of new blood vessels. *J Surg Res.* 2007; 137(1): 30–37. <https://doi.org/10.1016/j.jss.2006.05.041> PMID: 17084412

18. Blackwood KA, McKean R, Canton I, Freeman CO, Franklin KL, Cole D, et al. Development of biodegradable electrospun scaffolds for dermal replacement. *Biomaterials*. 2008; 29(21): 3091–3104. <https://doi.org/10.1016/j.biomaterials.2008.03.037> PMID: 18448164
19. Van der Veen VC, van der Wal MB, van Leeuwen MC, Ulrich MM, Middelkoop E. Biological background of dermal substitutes. *Burns*. 2010; 36(3): 305–321. <https://doi.org/10.1016/j.burns.2009.07.012> PMID: 19897310
20. Watanabe N, Ohashi K, Tatsumi K, Utoh R, Shim IK, Kanegae K, et al. Genetically modified adipose tissue-derived stem/stromal cells, using simian immunodeficiency virus-based lentiviral vectors, in the treatment of hemophilia B. *Hum Gene Ther*. 2013; 24(3): 283–294. <https://doi.org/10.1089/hum.2012.162> PMID: 23360488
21. Kato Y, Iwata T, Morikawa S, Yamato M, Okano T, Uchigata Y. Allogeneic transplantation of an adipose-derived stem cell sheet combined with artificial skin accelerates wound healing in a rat wound model of type 2 diabetes and obesity. *Diabetes*. 2015; 64(8): 2723–2734. <https://doi.org/10.2337/db14-1133> PMID: 25795216
22. Cerqueira MT, da Silva LP, Santos TC, Pirraco RP, Correlo VM, Reis RL, et al. Gellan gum-hyaluronic acid spongy-like hydrogels and cells from adipose tissue synergize promoting neoskin vascularization. *ACS Appl Mater Interfaces*. 2014; 6(22): 19668–19679. <https://doi.org/10.1021/am504520j> PMID: 25361388
23. Liu S, Zhang H, Zhang X, Lu W, Huang X, Xie H, et al. Synergistic angiogenesis promoting effects of extracellular matrix scaffolds and adipose-derived stem cells during wound repair. *Tissue Eng Part A*. 2011; 17(5–6): 725–739. <https://doi.org/10.1089/ten.TEA.2010.0331> PMID: 20929282
24. Kawamoto T, Shimizu M. A method for preparing 2- to 50-micron-thick fresh-frozen sections of large samples and undecalcified hard tissues. *Histochem Cell Biol*. 2000; 113(5): 331–339. PMID: 10883392
25. Chen YW, Scutaru TT, Ghetu N, Carasevici E, Lupascu CD, Ferariu D, et al. The effects of adipose-derived stem cell-differentiated adipocytes on skin burn wound healing in rats. *J Burn Care Res*. 2017; 38(1): 1–10. <https://doi.org/10.1097/BCR.000000000000466> PMID: 27893580
26. Loder S, Peterson JR, Agarwal S, Eboda O, Brownley C, DeLaRosa S, et al. Wound healing after thermal injury is improved by fat and adipose-derived stem cell isografts. *J Burn Care Res*. 2015; 36(1): 70–76. <https://doi.org/10.1097/BCR.000000000000160> PMID: 25185931
27. Huang SP, Huang CH, Shyu JF, Lee HS, Chen SG, Chan JY, et al. Promotion of wound healing using adipose-derived stem cells in radiation ulcer of a rat model. *J Biomed Sci*. 2013; 20: 51. <https://doi.org/10.1186/1423-0127-20-51> PMID: 23876213
28. Nambu M, Kishimoto S, Nakamura S, Mizuno H, Yanagibayashi S, Yamamoto N, et al. Accelerated wound healing in healing-impaired db/db mice by autologous adipose tissue-derived stromal cells combined with atelocollagen matrix. *Ann Plast Surg*. 2009; 62(3): 317–321. <https://doi.org/10.1097/SAP.0b013e31817f01b6> PMID: 19240532
29. Yu G, Floyd ZE, Wu X, Hebert T, Halvorsen YD, Buehrer BM, et al. Adipogenic differentiation of adipose-derived stem cells. *Methods Mol Biol*. 2011; 702: 193–200. https://doi.org/10.1007/978-1-61737-960-4_14 PMID: 21082403
30. De Francesco F, Tirino V, Desiderio V, Ferraro G, D'Andrea F, Giuliano M, et al. Human CD34/CD90 ASCs are capable of growing as sphere clusters, producing high levels of VEGF and forming capillaries. *PLoS One*. 2009; 4: e6537. <https://doi.org/10.1371/journal.pone.0006537> PMID: 19657392
31. Desiderio V, De Francesco F, Schiraldi C, De Rosa A, La Gatta A, Paino F, et al. Human Ng2+ adipose stem cells loaded in vivo on a new crosslinked hyaluronic acid-Lys scaffold fabricate a skeletal muscle tissue. *J Cell Physiol*. 2013; 228: 1762–1773. <https://doi.org/10.1002/jcp.24336> PMID: 23359523
32. Stellavato A, La Noce M, Corsuto L, Pirozzi AVA, De Rosa M, Papaccio G, et al. Hybrid Complexes of High and Low Molecular Weight Hyaluronans Highly Enhance HASCs Differentiation: Implication for Facial Bioremodelling. *Cell Physiol Biochem*. 2017; 44(3): 1078–1092. <https://doi.org/10.1159/000485414> PMID: 29179206
33. Pisciotta A, Bertoni L, Riccio M, Mapelli J, Bigiani A, La Noce M, et al. Use of a 3D Floating Sphere Culture System to Maintain the Neural Crest-Related Properties of Human Dental Pulp Stem Cells. *Front Physiol*. 2018; 9: 547. <https://doi.org/10.3389/fphys.2018.00547> PMID: 29892229
34. Spina A, Montella R, Liccardo D, De Rosa A, Laino L, Mitsiadis TA, et al. NZ-GMP Approved Serum Improve hDPSC Osteogenic Commitment and Increase Angiogenic Factor Expression. *Front Physiol*. 2016; 7: 354. <https://doi.org/10.3389/fphys.2016.00354> PMID: 27594842
35. Cao Y, Sun Z, Liao LM, Meng Y, Han Q, Zhao RC. Human adipose tissue-derived stem cells differentiate into endothelial cells in vitro and improve postnatal neovascularization in vivo. *Biochem Biophys Res Commun*. 2005; 332: 370–379. <https://doi.org/10.1016/j.bbrc.2005.04.135> PMID: 15896706

36. Lu F, Mizuno H, Uysal CA, Cai X, Ogawa R, Hyakusoku H. Improved viability of random pattern skin flaps through the use of adipose-derived stem cells. *Plast Reconstr Surg*. 2008; 121(1): 50–58. <https://doi.org/10.1097/01.prs.0000293876.10700.b8> PMID: 18176205
37. Rustad KC, Wong VW, Sorkin M, Glotzbach JP, Major MR, Rajadas J, et al. Enhancement of mesenchymal stem cell angiogenic capacity and stemness by a biomimetic hydrogel scaffold. *Biomaterials*. 2012; 33: 80–90. <https://doi.org/10.1016/j.biomaterials.2011.09.041> PMID: 21963148
38. Zografou A, Papadopoulos O, Tsigris C, Kavantzias N, Michalopoulos E, Chatzistamatiou T, et al. Autologous transplantation of adipose-derived stem cells enhances skin graft survival and wound healing in diabetic rats. *Ann Plast Surg*. 2013; 71: 225–32. <https://doi.org/10.1097/SAP.0b013e31826af01a> PMID: 23636118
39. Zonari A, Martins TM, Paula AC, Boeloni JN, Novikoff S, Marques AP, et al. Polyhydroxybutyrate-co-hydroxyvalerate structures loaded with adipose stem cells promote skin healing with reduced scarring. *Acta Biomater*. 2015; 17: 170–181. <https://doi.org/10.1016/j.actbio.2015.01.043> PMID: 25662911
40. Yun IS, Jeon YR, Lee WJ, Lee JW, Rah DK, Tark KC, et al. Effect of human adipose derived stem cells on scar formation and remodeling in a pig model: a pilot study. *Dermatol Surg*. 2012; 38: 1678–1688. <https://doi.org/10.1111/j.1524-4725.2012.02495.x> PMID: 22804839
41. Li WY, Huang EY, Dudas M, Kaartinen V, Warburton D, Tuan TL. Transforming growth factor-beta3 affects plasminogen activator inhibitor-1 expression in fetal mice and modulates fibroblast-mediated collagen gel contraction. *Wound Repair Regen*. 2006; 14: 516–525. <https://doi.org/10.1111/j.1743-6109.2006.00158.x> PMID: 17014662
42. Chalmers RL. The evidence for the role of transforming growth factor-beta in the formation of abnormal scarring. *Int Wound J*. 2011; 8: 218–223. <https://doi.org/10.1111/j.1742-481X.2011.00771.x> PMID: 21449929
43. Lin YC, Grahovac T, Oh SJ, Ieraci M, Rubin JP, Marra KG. Evaluation of a multi-layer adipose-derived stem cell sheet in a full-thickness wound healing model. *Acta Biomater*. 2013; 9(2): 5243–5250. <https://doi.org/10.1016/j.actbio.2012.09.028> PMID: 23022891